


Optical Phase/Frequency Demodulation Using Polarization-Maintaining Fiber Bragg Gratings

Dipen Barot , *Member, IEEE*, Rui Zhou, *Student Member, IEEE*, and Lingze Duan , *Senior Member, IEEE*

Abstract—Conventional techniques for demodulating phase/frequency-modulated (PM/FM) optical signals either require a sophisticated frequency-stable laser or employ a discriminator with poor characteristics. Here, we present a simple, compact, and robust technique featuring high linearity over a wide bandwidth and low background noise. Our technique exploits the reflection characteristics of fiber Bragg gratings written in polarization-maintaining fibers to create a frequency discriminator, which is able to convert PM/FM signals into intensity-modulated (IM) signals. A simple theoretical analysis is presented to highlight the advantages of the scheme. Experimentally, the transfer characteristics of the demodulator are characterized, yielding a linear FM-to-IM conversion slope of 1.238 mV/Hz in a 0.2-nm (~ 25 GHz) bandwidth. Highly linear operation up to an FM-modulation index of 1.2 has been achieved. Background-free operation is shown by demonstrating negligible carrier leakage and a 10-dB IM rejection. Finally, high fidelity in demodulating arbitrary PM/FM optical signals is demonstrated with a correlation coefficient of 0.99 and a confidence of almost 100%. This simple yet efficient technique can potentially find applications in optical communications, microwave photonics and radar/lidar technologies.

Index Terms—Frequency modulation, lidar, microwave measurements, microwave photonics, optical communications, phase modulation, wideband measurements.

I. INTRODUCTION

PHASE-MODULATED and frequency-modulated (PM/FM) optical signals find use in applications such as optical communications, optical frequency metrology, frequency-modulated continuous wave (FMCW) lidar, optical sensing, and frequency modulation spectroscopy owing to their many advantages over intensity-modulated (IM) signals. In optical communications, for instance, PM/FM microwave photonic links (MPLs) are considered as promising alternatives to optical IM-MPLs because of their reduced fiber

Manuscript received 8 May 2022; revised 5 August 2022; accepted 24 August 2022. Date of publication 30 August 2022; date of current version 16 November 2022. This work was supported by the National Science Foundation under Grants ECCS-1254902 and ECCS-1606836. (*Corresponding author: Dipen Barot.*)

Dipen Barot was with the Department of Physics and Astronomy, The University of Alabama in Huntsville, Huntsville, AL 35899 USA. He is now with the National Institute of Standards and Technology, Boulder, CO 80305 USA, and also with the University of Colorado, Boulder, CO 80302 USA (e-mail: diba7095@colorado.edu).

Rui Zhou and Lingze Duan are with the Department of Physics and Astronomy, The University of Alabama in Huntsville, Huntsville, AL 35899 USA (e-mail: rz0006@uah.edu; ld0003@uah.edu).

Color versions of one or more figures in this article are available at <https://doi.org/10.1109/JLT.2022.3202788>.

Digital Object Identifier 10.1109/JLT.2022.3202788

nonlinear effects, multichannel operation capability, higher signal-to-noise ratio (SNR), and higher modulation efficiency [1], [2], [3]. In ranging and detection, FMCW lidar offers higher sensitivity and virtually interference-free operation when compared to conventional time-of-flight lidar [4]. In all these applications, a way to efficiently demodulate the PM/FM signal is necessary for extracting the desired information. In frequency-modulation spectroscopy, for example, PM/FM signals are converted into IM signals by the atomic or molecular absorption spectrum of the sample. The IM signals are then detected using simple photodetection. For optical communications, a scheme with a high bandwidth and good linearity is critical in ensuring that transmitted data signals are recovered with high fidelity at the receiver end.

Various techniques have been demonstrated for optical PM/FM demodulation. They can be generally categorized as either coherent-demodulation techniques (CDT) or incoherent-demodulation techniques (IDT). In CDT, the PM/FM signal beats against a frequency-stabilized local oscillator in the optical domain and the derived heterodyne signal is analyzed using radio-frequency (RF) techniques [5], [6], [7]. Due to the stringent requirement of a frequency-stable local oscillator, CDT are generally complex, hard to scale up, and difficult to use in practical applications. In contrast, an IDT detects PM/FM without a frequency-stable local oscillator. Instead, IDT converts PM/FM signals to IM signals by employing a phase/frequency-discriminator, whose intensity-versus-frequency slope sets the linearity and the bandwidth of the demodulator. Among IDT schemes, Mach-Zehnder interferometers (MZI) are commonly used for demodulating PM/FM signals [6], [7], [8]. The drawback of these interferometer-based schemes lies in the trade-off between SNR and bandwidth due to delay restrictions. The nonlinear nature of an interferometer response also introduces inter-modulation products in the output, which reduces the demodulation fidelity. Moreover, MZI-based schemes often need to be biased around a quadrature point, which may need to be stabilized against various instabilities in the system.

To overcome the linearity limitation of conventional MZI-based schemes, ring-assisted MZI has been proposed [9]. It offers a slightly improved linearity, but the improvement comes at the cost of a complicated quadrature bias requirement in addition to increased system loss due to the integration of ring resonators in the MZI arms. IDTs based on Sagnac interferometers have also been proposed [10]. Such schemes are limited not only by the requirement of fixing the quadrature bias point along a nonlinear transmission spectrum but also by the instabilities caused

by long fibers and complicated angle settings among several polarization controllers. Fabry-Perot interferometers (FPI) have been used as well to demodulate PM/FM signals [11], [12], although they face similar challenges and limitations as the MZIs. More recently, a self-heterodyne interferometric technique has been proposed [13]. This method requires precise calibration of the delay time and needs phase extraction using a vector signal analyzer with an accuracy of ± 3 degree, which is quite stringent for practical applications. Also, such an interferometric approach suffers from a large background noise unless a second quadrature point with an exactly opposite slope is used in a balanced-detection scheme.

IDTs based on dispersive optical elements such as fiber Bragg gratings (FBG) have also attracted a lot of interest in recent years [14]. Although simple and robust, such schemes are often susceptible to background noises due to the non-zero bias point on the slopes of the FBG reflection peak [15]. A dual-FBG scheme with two complementary FBGs is under consideration to remove the background noise [16]. However, it suffers from nonlinearity issues, especially at low modulation rates [17]. Meanwhile, chirped FBGs have also been used in IDT schemes. But such a method encounters a tight fabrication need to ensure the precise nonlinear chirp rate of the gratings [18]. IDTs using birefringent crystals are also a potential approach under investigation [19]. This scheme is compact, rigid, and less restricted in delay requirements due to a common light path. But it requires long crystals for low modulation rates, which introduces angular limitations due to alignment issues of free-space optics [20].

Overall, despite a lot of past effort, there is still a need for a simple and robust FM/PM demodulation scheme that can achieve linear, wideband, and background-free operation. Here, we present a novel fiber-optic technique with such capabilities. Our technique combines the advantages of FBGs and birefringent crystals by employing an FBG fabricated in a polarization maintaining (PM) fiber, i.e., a PM-FBG. Such a combination allows the demodulator to enjoy the low cost and compactness of an FBG while benefitting from the rigidity and the common optical path of a birefringent material [21]. Because of the birefringence property of the PM fiber, a single FBG results in two identical reflection peaks with a slight wavelength offset along the two orthogonal polarizations, alleviating the burden of fabricating two identical FBGs. The double-peak profile also provides a natural quadrature point with equal and opposite slopes. This allows a PM-FBG to perform background-free linear operations.

II. PRINCIPLE OF OPERATION

A. Basics of PM/FM Signals

In general, a sinusoidal carrier with a constant amplitude and a time-varying phase can be mathematically described by [22]

$$x(t) = A_c \exp[j\theta(t)] = A_c \exp\{j[2\pi f_c t + \phi(t)]\}, \quad (1)$$

where A_c is carrier amplitude, $\theta(t)$ is total instantaneous angle, f_c is carrier frequency, and $\phi(t)$ is time-dependent phase angle. If the phase is subject to a modulation, it can be further expressed

as

$$\phi(t) = 2\pi K_f \int_0^t m(\tau) d\tau, \quad (2)$$

where K_f is frequency sensitivity of the modulator and $m(\tau)$ is the modulation signal. The instantaneous frequency of the signal $x(t)$ is defined as

$$f(t) \equiv \frac{1}{2\pi} \dot{\theta}(t) = f_c + K_f m(t). \quad (3)$$

Note from (2) and (3) that frequency modulation and phase modulation connect through a linear relationship. Also, when the frequency of a carrier is modulated by $m(t)$, it is evident that the phase is being modulated by the time-integral of $m(t)$. Because of the simple relations of (2) and (3), all analytical and experimental results of FM signals can easily be applied to PM signals through the time-integral relation. Henceforth, all of the following discussions only focus on FM signals.

B. FM Demodulator Characteristics

Since an arbitrary modulation signal can be decomposed into a collection of single-frequency components via Fourier transform, it is worthwhile to take a closer look at the so-called tone modulation, where $m(\tau)$ takes the form of a sinusoidal function $m(\tau) = A_m \cos(2\pi f_m \tau)$, with A_m being the modulation amplitude and f_m representing the modulation frequency. Equation (1) can be rewritten as

$$x(t) = A_c \exp(j2\pi f_c t) \cdot \exp[j\beta \sin(2\pi f_m t)], \quad (4)$$

where $\beta = K_f A_m / f_m$ is commonly known as the frequency modulation index. By defining peak FM frequency deviation $\Delta f = K_f A_m$, modulation index can also be expressed as $\beta = \Delta f / f_m$. Expanding the second exponential term in (4) into an infinite series yields [17]

$$x(t) = A_c \sum_{n=-\infty}^{+\infty} J_n(\beta) \exp[j2\pi (f_c + n f_m) t], \quad (5)$$

where $J_n(\beta)$ is Bessel function of the first kind of order n and the argument β .

Fig. 1(a) and (b) show a typical single-tone FM signal in the time and the frequency domains, respectively. In the time domain, f_c is found to vary at a rate of f_m , as shown in Fig. 1(a). In the frequency domain, the spectrum of the signal has infinite sidebands around f_c at integer multiples of f_m , as shown in Fig. 1(b). Fig. 1(c) and (d) represent a multi-tone FM signal in time and frequency, respectively. Fig. 1(c) shows that f_c appears to vary arbitrarily in time. The multi-tone nature of the modulating signal becomes clear in the frequency domain, where all the f_m (i.e., f_{m1} , f_{m2} and f_{m3}) making up the modulating signal along with their integer multiples can be seen around f_c , as shown in Fig. 1(d).

From the demodulation viewpoint, an ideal demodulator must faithfully retrieve the modulating signal without distortion. To characterize practical demodulators, certain parameters must be defined. One important parameter is *linearity*, which is defined

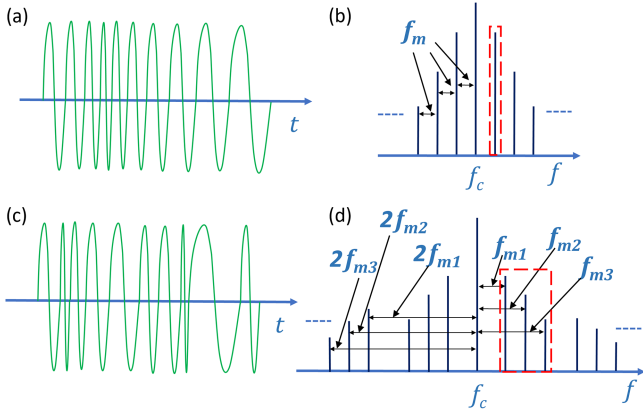


Fig. 1. Single-tone frequency modulated carrier signal in (a) the time domain and (b) the frequency domain, and multi-tone frequency modulated carrier signal in (c) the time domain and (d) the frequency domain.

as the linear variation in the output of a demodulator with respect to the frequency displacement of an unmodulated signal. Another key parameter is *background noise*, which is used to characterize the leakage of the carrier signal through the demodulator and the response to IM of the FM signal. Both factors degrade the performance of a demodulator by lowering the SNR at the output. Ideally, an FM demodulator should have perfect linearity as well as zero background noise.

C. Operating Principle of PM-FBG Based FM Demodulator

Our technique exploits the reflection characteristics of PM-FBG for converting FM to IM. The reflection spectrum from a PM-FBG features two resonance peaks [23]. Their wavelengths are given by

$$\lambda_s = 2\Lambda n_{eff}^s \text{ and } \lambda_f = 2\Lambda n_{eff}^f, \quad (6)$$

where Λ is the grating period, λ_s (λ_f) is the Bragg wavelength, and n_{eff}^s (n_{eff}^f) is the effective refractive index for the polarization component along the slow (fast) axis [8]. Note that n_{eff}^s and n_{eff}^f are nearly equal. Thus, the two reflection peaks are relatively close with an overlapping region.

Given this basic concept of PM-FBG, here is how the proposed demodulator works: A proper PM-FBG is chosen so that its two resonance peaks cross near their 3 dB points (for maximum slope), as shown in Fig. 2(a). An ideal optical oscillator with a single frequency is first tuned to the crossover wavelength between the two Bragg reflection peaks, as illustrated by the left panel of Fig. 2(a). The polarization of the injected optical carrier is adjusted so that an equal amount of optical power is reflected by the PM-FBG along its fast and slow axes. The two orthogonally polarized reflection signals are separately detected, and the detector outputs are subtracted from each other to create a *null* (i.e., balanced photodetection (BPD)), as shown in the right panel of Fig. 2(a). This effectively creates a quadrature point. When the frequency of the optical carrier is dislocated from the crossover wavelength, the reflected powers along the fast and the slow axes change toward opposite directions due to the opposite signs of their corresponding reflectivity slopes.

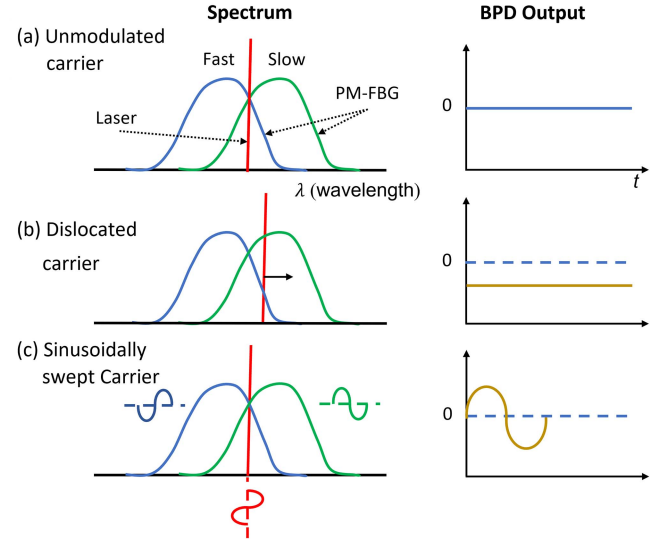


Fig. 2. Operating principle of the PM-FBG based PM/FM discriminator: The reflection spectrum of PM-FBG relative to the laser (left) and the corresponding output of the BPD (right) for (a) ideal oscillator, (b) dislocated oscillator, and (c) sinusoidally swept oscillator.

This allows the BPD to generate a large response, as shown in the right panel of Fig. 2(b). Moreover, when the frequency of the optical carrier is modulated near the crossover wavelength, as figuratively shown in Fig. 1(a) and (c) and conceptually depicted in Fig. 2(c), the reflected optical intensities along the fast and the slow axes also vary periodically but with a 180-degree phase difference. This leads to a large, background-free response at the output of the BPD. In essence, the above scheme allows the PM-FBG to serve as an optical frequency discriminator, which in turn performs FM demodulation.

III. THEORY

This section presents a simplified theoretical analysis of our technique. We again consider a tone-modulated optical carrier described by (5) as the input to the demodulator. Its Fourier transform yields

$$X(f) = \frac{A_c}{2} \sum_{n=-\infty}^{n=+\infty} J_n(\beta) \delta(f - f_c - n f_m) \quad (7)$$

Let us assume that the carrier frequency of (7) is tuned at the crossover point of PM-FBG and its polarization is adjusted such that a null is detected at the output of the BPD when no modulation is applied, as shown in Fig. 2(a). In this situation, both polarization components of the input are reflected according to the corresponding FBG reflection profiles.

First, consider the reflection along the fast axis. Since the signal is located near the middle of the falling slope, a linear transfer function can be assumed and written as

$$H^{fast}(f) = r(f) e^{-j2\pi f \tau_d} \quad (8)$$

where $r(f)$ is a frequency dependent reflection coefficient along the fast axis of the PM-FBG, τ_d is the group delay induced by

the FBG. The reflected signal along the fast axis is given by

$$X^{fast}(f) = X(f)H^{fast}(f) = \frac{A_c}{2} \sum_{n=-\infty}^{n=+\infty} J_n(\beta) r(f_c + n f_m) e^{-j(2\pi(f_c + n f_m)\tau_d)} \delta(f - (f_c + n f_m)) \quad (9)$$

Similarly, the reflected field along the slow axis can be derived as

$$X^{slow}(f) = X(f)H^{slow}(f) = \frac{A_c}{2} \sum_{n=-\infty}^{n=+\infty} J_n(\beta) r^*(f_c + n f_m) e^{-j(2\pi(f_c + n f_m)\tau_d)} \delta(f - (f_c + n f_m)) \quad (10)$$

where $r^*(f)$ is the frequency dependent reflection coefficient along the slow axis. Now, when the reflected signals along the two polarization axes are separately detected by the two photodetectors of the BPD, the generated photo currents are proportional to the incident optical power P_{out} . For simplicity, in the following, we consider the case of narrowband FM, where only three terms ($n = 0$ and ± 1) exist in (9) and (10) and the two sidebands are much smaller than the carrier, A tedious but straightforward derivation yields the following expressions for the Fourier components of the photo currents generated by the two photodetectors,

$$\begin{aligned} i^{fast}(f) &\propto F \left\{ < P_{out}^{fast}(t) > \right\} \\ &= d_0 \delta(f) + d_1 f_m \frac{dr}{df} \delta(f - f_m) e^{-j2\pi f_m \tau_d} \\ &\quad + d_1 f_m \frac{dr}{df} \delta(f + f_m) e^{j2\pi f_m \tau_d} \end{aligned} \quad (11)$$

$$\begin{aligned} i^{slow}(f) &\propto F \left\{ < P_{out}^{slow}(t) > \right\} \\ &= d_0 \delta(f) + d_1 f_m \frac{dr^*}{df} \delta(f - f_m) e^{-j2\pi f_m \tau_d} \\ &\quad + d_1 f_m \frac{dr^*}{df} \delta(f + f_m) e^{j2\pi f_m \tau_d} \end{aligned} \quad (12)$$

where $F\{\}$ and $< >$ indicates the Fourier transform and time average, respectively. Note that only the zeroth-order (DC) and the first-order (f_m) terms are kept in these relations. The DC-term is scaled by the coefficient d_0 and is due to the reflected optical carrier. The two first-order terms are caused by the beating between the sidebands and the carrier, while d_1 is a constant of proportionality. The terms dr/df and dr^*/df are derived by linearly expanding $r(f)$ and $r^*(f)$ around f_c ,

$$r(f_c - f_m) = r_c - f_m \frac{dr}{df}, \quad (13)$$

$$r^*(f_c - f_m) = r_c^* - f_m \frac{dr^*}{df}, \quad (14)$$

with r_c and r_c^* representing the optical reflectivities at the carrier frequency along the fast and the slow axes, respectively. Now,

taking the difference between (11) and (12), we obtain the output of the BPD

$$\begin{aligned} y(f) &\propto i^{fast}(f) - i^{slow}(f) \\ &= d_1 f_m \left\{ \frac{dr}{df} - \frac{dr^*}{df} \right\} \delta(f - f_m) e^{-j2\pi f_m \tau_d} \\ &\quad + d_1 f_m \left\{ \frac{dr}{df} - \frac{dr^*}{df} \right\} \delta(f + f_m) e^{j2\pi f_m \tau_d} \end{aligned} \quad (15)$$

Since $r(f)$ and $r^*(f)$ have opposite slopes around the crossover point, we can assume the following relation

$$\frac{dr}{df} = -\frac{dr^*}{df}. \quad (16)$$

Inserting (16) into (15) yields

$$\begin{aligned} y(f) &\propto 2d_1 f_m \frac{dr}{df} \delta(f - f_m) e^{-j2\pi f_m \tau_d} \\ &\quad + 2d_1 f_m \frac{dr}{df} \delta(f + f_m) e^{j2\pi f_m \tau_d} \end{aligned} \quad (17)$$

Equation (16) shows that carrier leakage (*i.e.*, the d_0 term), which is responsible for background noise, is removed in our technique. The factor of 2 leading the d_1 terms also indicates that the amplitude of the demodulated signal is *doubled* by the PM-FBG (*i.e.*, a 3-dB improvement) in comparison with using a single FBG. Furthermore, the fact that $y(f = f_m) \propto f_m$ indicates that the output of the demodulator is proportional to the *time* derivative of the modulation signal, which is a linear operation. It is important to point out from the above analysis that any nonlinearity in reflectivity, which is neglected in above simplified analysis, will give rise to nonlinear responses in the output by introducing harmonic and IMD distortion terms.

IV. EXPERIMENTAL SETUP

An experiment has been set up to verify the performance of a PM-FBG based FM demodulator. A layout of the experimental system is shown in Fig. 3(a), where the components of the demodulator are encircled by the dashed line. The PM-FBG is fabricated on a PANDA-type PM fiber. It has two Bragg reflection peaks about 0.6 nm apart, with each peak having a 0.4-nm full width at half maximum (FWHM) (see Fig. 3(b)). A tunable external-cavity diode laser operating near 1550 nm serves as the light source. Its wavelength is tuned to the crossover wavelength of the two Bragg peaks, as shown in Fig. 3(b). The laser output passes through an isolator before entering a polarization controller (PC). The polarization controller is used to set the polarization state of the light. A polarization-maintaining 50:50 coupler takes the output of the PC, feeds it into the PM-FBG, and directs the reflected power toward the output. A fiber-coupled polarization beam splitter splits the two orthogonal polarization modes in the output, feeding them into the two photodiodes of a balanced photoreceiver (Thorlabs PDB 440C), which provides a transimpedance gain of 5.1×10^4 V/A. The input of the demodulator is PM/FM-modulated via an electro-optic modulator (EOM), which is driven by an RF driver. All the fibers and fiber connectors after the polarization controller are PM type so that

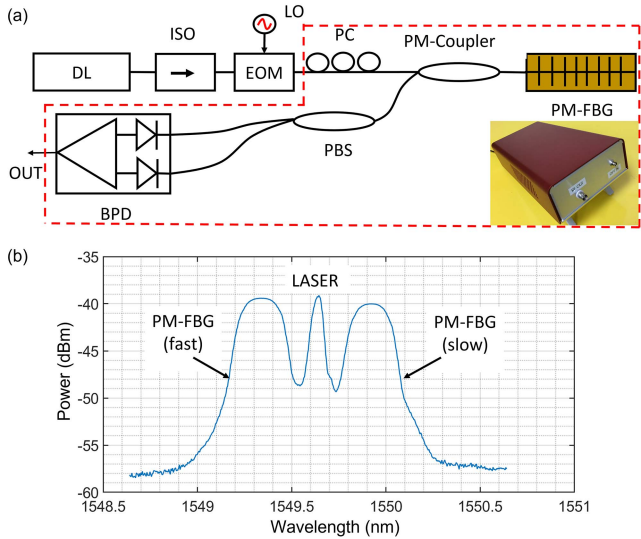


Fig. 3. (a) Schematic of the experimental setup for testing the PM-FBG demodulator. DL: diode laser, EOM: electro-optic phase modulator, ISO: fiber-coupled isolator, PBS: polarization beam splitter, PC: polarization controller, PM-Coupler: polarization-maintaining coupler (Inset: A benchtop module of the demodulator). (b) A measured FBG-reflection spectrum when the laser wavelength is tuned to the crossover point between two PM-FBG Bragg peaks.

the polarization state is preserved. The inset in Fig. 3(a) shows the picture of an actual module of the demodulator, which is housed in a 300 mm × 150 mm × 83 mm instrumentation box with optical input and RF output ports.

V. RESULTS

Linearity and wideband transfer characteristics are critical for any FM demodulator. To find out the transfer characteristics of the PM-FBG demodulator, the wavelength of the tunable diode laser is swept within the reflection spectrum of the PM-FBG, and the reflected light in the two orthogonal polarization states are separately detected. The resulting traces are shown in Fig. 4(a), where two distinctive reflection peaks with a crossover wavelength of 1549.7 nm can be clearly seen. Fig. 4(b) shows the balanced output of the BPD. It is evident that good linear operation has been obtained in a 0.2-nm wavelength (1549.6 nm to 1549.8 nm) range near the crossover point, which corresponds to a bandwidth of ~ 25 GHz. The slope of the linear section is about 15.467 V/nm, indicating a FM-to-IM conversion efficiency of 1.238 mV/Hz. Moreover, Fig. 4(b) also suggests that the quadrature point (1549.7 nm) corresponds to zero output voltage, i.e., no carrier leakage.

Additional tests of linearity are performed by measuring the demodulated signal level versus the FM modulation index. An increase in the FM modulation index results in an increase in the carrier displacement from the quadrature point. Fig. 5 shows the peak-to-peak voltage at the output of BPD as the FM modulation index at the input of the demodulator is increased. Highly linear operation is evidently achieved. Currently, the modulation frequency in our experiment (1 MHz) is limited by the speed of the BPD. In principle, it can reach as high as 12.5 GHz, limited only by the linear region of the PM-FBG.

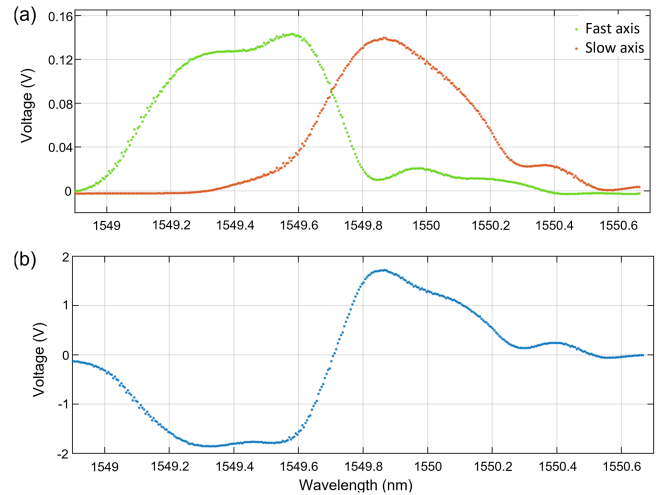


Fig. 4. Experimental traces of (a) two reflection peaks of PM-FBG when the input is appropriately polarized and frequency-swept across their profiles, and (b) the BPD output when two orthogonal polarizations are separately detected.

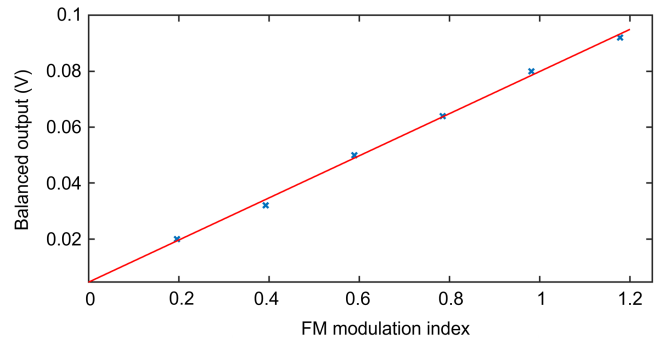


Fig. 5. Demodulator output (peak-to-peak voltage) vs. FM modulation index. Solid (red) line represents linear fitting.

The background noise in the output of an FM demodulator mainly comes from carrier leakage and the unwanted response to IM. To measure the IM response of our FM demodulator, we purposely applied IM along with FM by placing an intensity modulator in series with the EOM. A small fraction (10%) of the intensity-modulated light is measured with a separate photodiode, and the rest of the light is applied to the FM demodulator. Fig. 6 shows the measured response in both the time and the frequency domains. In Fig. 6(a), the dashed (red) trace shows the applied IM to the laser at 100 kHz with a 10% modulation depth, and the solid (blue) trace depicts the balanced output of the FM demodulator when a 2-MHz square wave is applied to the EOM. It can be seen that the square-wave FM signal is nicely recovered with a near-zero DC bias, indicating negligible carrier leakage while preserving the square waveform. To better quantify the IM rejection of the demodulator, we measured the FFT of the demodulator output. As shown in Fig. 6(b), the FFT of the demodulated signal contains 100-kHz IM sidebands around the 2-MHz FM modulation peak. Further measurement shows that the IM sidebands are 36 dB below the FM carrier peak. Meanwhile, based on the 10% IM modulation depth, it is straightforward to estimate that the IM sidebands should be 26 dB below the carrier peak, as marked in Fig. 6(b) with the dots

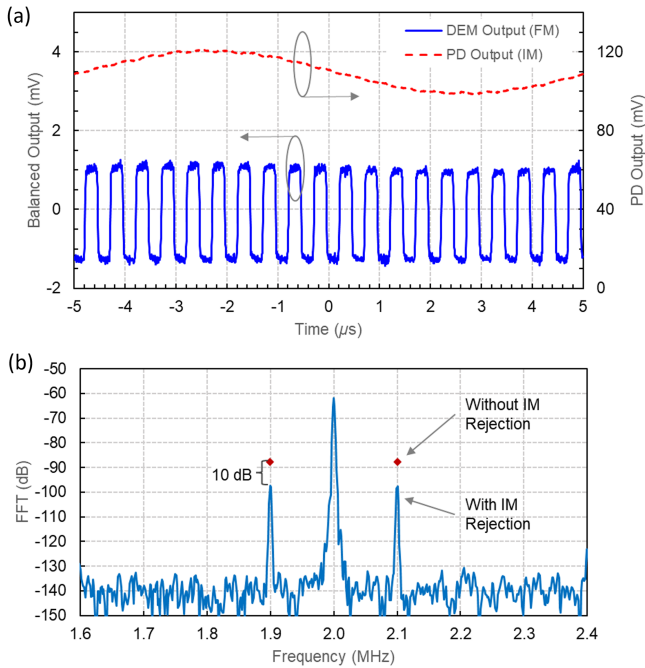


Fig. 6. Demonstration of IM rejection (or background rejection) by the PM-FBG demodulator. (a) Time domain traces of the 100-kHz IM signal (dashed) and the 2-MHz FM signal. The latter is recovered using the PM-FBG demodulator. (b) FFT trace of the recovered FM signal near its fundamental frequency at 2 MHz. The measured IM sidebands are 36 dB below the carrier, approximately 10 dB lower than the theoretical sideband peaks if IM rejection is absent.

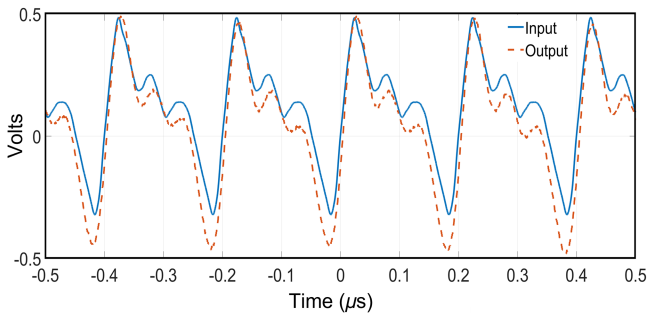


Fig. 7. A comparison between the FM driving signal (solid) and the recovered signal (dashed) at the output of the PM-FBG demodulator.

(red). This suggests that the demodulator introduces a 10-dB IM rejection, which clearly demonstrates the advantage of the differential detection scheme.

The recovery of frequency modulating signal with high fidelity is another crucial aspect for FM demodulators. To examine the fidelity of the PM-FBG demodulator, an arbitrary periodic signal at a frequency of 5 MHz is applied to the EOM, and the recovered FM signal is compared with the original driving signal as shown in Fig. 7. Evidently, the recovered signal (dashed) preserves the shape of input signal and contains all the key features with a very mild deviation. The computed correlation coefficient between the applied modulation signal and the recovered signal is 0.9901 with a confidence of almost 100% (p -value = 0), demonstrating a very high fidelity for FM demodulation. Note that the average voltage of recovered signal is near zero,

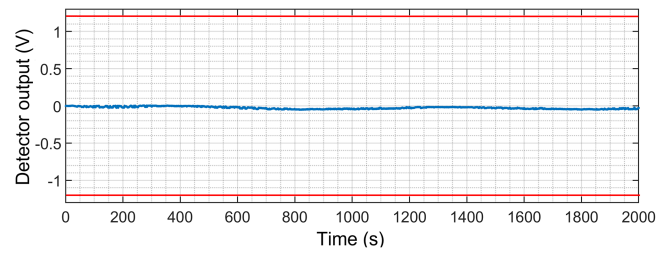


Fig. 8. Measurement of the BPD output when the optical carrier is initialized at the quadrature point and has no FM applied, demonstrating the long-term stability of the demodulator.

showing negligible carrier leakage. The slight distortion in the recovered signal is likely caused by polarization fluctuations due to environmental effects and/or slight dislocation of optical carrier from the crossover point. With a simple temperature control of the demodulator enclosure, these factors can be further improved.

VI. DISCUSSION

Long-term stability is a critical metric for FM demodulators. In the case of PM-FBG, temperature variations can lead to Bragg wavelength shifts and polarization state fluctuations. Both of these effects cause the BPD output to drift away from the null without carrier modulation. Such drift may increase background noise and introduce distortion in the output. To verify the tolerance of our demodulator against temperature fluctuations, we monitored the BPD output without any input FM signals in a normal lab environment for long periods of time. Fig. 8 shows the BPD output over 2000 seconds upon an initial optimization of the carrier frequency. It is found that, even with a random drift over time, the BPD output remains close to zero within about 50 mV for extended periods of time (sometimes hours). This is in comparison with the maximum output range from the BPD, which is marked in Fig. 8 by the straight lines near the top and the bottom. The result shows that the PM-FBG demodulator can maintain good stability under a reasonably controlled environment.

Another factor that affects the performance of a demodulator is frequency noise. Frequency noise may come from either the input laser source or the transmission medium. Specifically, frequency noise introduces undesired sweeping of the carrier frequency near the quadrature point, which is indistinguishable from the desired FM signal. Frequency noise of the input laser source can be mitigated by using a low-noise laser source stabilized against a frequency reference. On the other hand, frequency noise introduced by the transmission medium can be removed by using passive compensation techniques (e.g., dispersion compensation) before demodulation.

Although the technique presented here is for FM/PM demodulation, it may also find applications in numerous other contexts. For example, it can be used for characterizing the frequency noise of a continuous-wave laser because it effectively provides an optical frequency discrimination. Moreover, our technique

might also be used as an efficient optical frequency-to-voltage converter because of its linearity and large bandwidth.

VII. CONCLUSION

We present here a simple, compact, and robust technique for demodulating PM/FM optical signals. It features high linearity, large bandwidth, and background-free operation. A simple frequency-domain analysis is presented as the theoretical background. The analysis reveals that the proposed technique can provide background-free operation with a 3-dB improvement in demodulated amplitude when compared with the single-FBG scheme. Experimentally, linear transfer characteristics over a frequency range of 25 GHz is demonstrated with a slope of 1.238 mV/Hz. A basic test of linearity is undertaken for a tone modulated signal, resulting in excellent performance over a 1.2-MHz bandwidth (frequency detuning). Carrier leakage and intensity modulation (IM), which corrupt the performance of FM demodulators, have been investigated. Near-zero DC bias in the output demonstrates negligible carrier leakage. A 10-dB IM rejection has also been achieved. A case study on demodulation fidelity shows excellent agreement between the demodulated signal and the original FM driving signal, with a correlation coefficient of 0.99 and a confidence of almost 100%. Discussions are made on several factors affecting the performance of the technique as well as the corresponding mitigation strategies. It is our hope that this work opens up a new avenue toward compact and low-cost optical PM/FM demodulators.

REFERENCES

- [1] C. H. Cox, III, *Analog Optical Links: Theory and Practice*. New York, NY, USA: Cambridge Univ. Press, 2004.
- [2] V. J. Urick, K. J. Williams, and J. D. McKinney, *Fundamental of Microwave Photonics*. Hoboken, NJ, USA: Wiley, 2015.
- [3] J. M. Wyrwas and M. C. Wu, "Dynamic range of frequency modulated direct detection analog fiber optic links," *J. Lightw. Technol.*, vol. 27, no. 24, pp. 5552–5562, Dec. 2009.
- [4] M.-C. Amann, T. M. Bosch, M. Lescure, R. A. Myllylae, and M. Rioux, "Laser ranging: A critical review of unusual techniques for distance measurement," *Opt. Eng.*, vol. 40, no. 1, pp. 10–19, Jan. 2001.
- [5] J. M. Kahn and K.-P. Ho, "Spectral efficiency limits and modulation/detection techniques for DWDM systems," *IEEE J. Sel. Topics Quantum Electron.*, vol. 10, no. 2, pp. 259–272, Mar./Apr. 2004.
- [6] W. V. Sorin, K. W. Chang, G. A. Conrad, and P. R. Hernday, "Frequency domain analysis of an optical FM discriminator," *J. Lightw. Technol.*, vol. 10, no. 6, pp. 787–793, Jun. 1992.
- [7] B. Dingel and N. Madamopoulos, "Optical frequency discriminator with ultrahigh-amplitude-and-phase linearity for frequency-modulated microwave photonic links," in *Proc. IEEE Photon. Conf.*, 2016, pp. 25–26.
- [8] B. Dingel, "Dual-slope linear optical frequency discriminator for flexible, high-performance frequency modulated direct detection (FM-DD) microwave photonics links," in *Proc. 26th Wireless Opt. Commun. Conf.*, Newark, NJ, USA, 2017, pp. 1–4.
- [9] X. Xie, J. Khurgin, J. Kang, and F.-S. Choa, "Ring-assisted frequency discriminator with improved linearity," *IEEE Photon. Technol. Lett.*, vol. 14, no. 8, pp. 1136–1138, Aug. 2002.
- [10] G. Chen, J. U. Kang, and J. B. Khurgin, "Frequency discriminator based on ring-assisted fiber sagnac filter," *IEEE Photon. Technol. Lett.*, vol. 17, no. 1, pp. 109–111, Jan. 2005.
- [11] P. Tremblay and R. Ouellet, "Frequency response of a Fabry-Perot interferometer used as a frequency discriminator," *IEEE Trans. Instrum. Meas.*, vol. 40, no. 2, pp. 204–207, Apr. 1991, doi: [10.1109/TIM.1990.1032916](https://doi.org/10.1109/TIM.1990.1032916).
- [12] E. Bava, G. Galzerano, and C. Svelto, "Fabry-Perot frequency discriminators: Sensitivity, amplitude noise immunity and noise limits," in *Proc. 17th IEEE Instrum. Meas. Technol. Conf.*, 2000, vol. 2, pp. 733–737.
- [13] H. Tsuchida, "Waveform measurement technique for phase/frequency-modulated lights based on self-heterodyne interferometry," *Opt. Exp.*, vol. 25, no. 5, pp. 4793–4799, Feb. 2017.
- [14] F. Zeng and J. Yao, "Frequency domain analysis of fiber Bragg grating based phase modulation to intensity modulation conversion," in *Proc. Photon. Appl. Nonlinear Opt., Nanophotonics, Microw. Photon.*, Toronto, Canada, 2005, vol. 5971, pp. 594–601.
- [15] T. G. Ulmer, "Distortion in angle-modulated links induced by ripple in fiber-Bragg-grating reflectance and delay characteristics," *J. Lightw. Technol.*, vol. 21, no. 12, pp. 3226–3236, Dec. 2003.
- [16] T. E. Darcie, J. Zhang, P. F. Driessen, and J. J. Eun, "Demonstration of a class-B microwave-photonic link using optical frequency modulation and complementary fiber-Bragg-grating discriminators," in *Proc. Opt. Fiber Commun. Conf. Nat. Fiber Opt. Eng. Conf.*, Anaheim, CA, USA, 2006, pp. 1–3.
- [17] P. F. Driessen, T. E. Darcie, and J. Zhang, "Analysis of a class-B microwave-photonic link using optical frequency modulation," *J. Lightw. Technol.*, vol. 26, no. 15, pp. 2740–2747, Aug. 2008.
- [18] X. Xie, J. B. Khurgin, J. U. Kang, and F. S. Choa, "Compact linearized optical FM discriminator," *IEEE Photon. Technol. Lett.*, vol. 14, no. 3, pp. 384–386, Mar. 2002.
- [19] I. P. Kaminow, "Balanced optical discriminator," *Appl. Opt.*, vol. 3, no. 4, pp. 507–510, Apr. 1964.
- [20] S. E. Haris, "Conversion of FM light to AM light using birefringent crystals," *Appl. Phys. Lett.*, vol. 2, no. 3, pp. 47–49, Feb. 1963.
- [21] D. Barot and L. Duan, "Optical frequency discriminator based on polarization-maintaining fiber Bragg gratings," in *Proc. Conf. Lasers Electro-Opt.*, San Jose, USA, 2020, Paper JTu2G.8.
- [22] D. Barot and L. Duan, "Laser frequency analysis aided by electronic frequency dividers," *J. Lightw. Technol.*, vol. 36, no. 12, pp. 2524–2530, Jun. 2018.
- [23] D. Barot, G. Wang, and L. Duan, "High-resolution dynamic strain sensor using a polarization maintaining fiber Bragg grating," *IEEE Photon. Technol. Lett.*, vol. 31, no. 9, pp. 709–712, May 2019.

Dipen Barot (Member, IEEE) received the Ph.D. degree in optical science and engineering from the University of Alabama, Huntsville, AL, USA, in 2019. He is currently a Postdoctoral Researcher with the Department of Physics, National Institute of Standards and Technology, University of Colorado Boulder, Boulder, CO, USA. His research interests include ultrafast optics, ultra-stable narrow linewidth optical sources, and fiber optic sensing. He was the recipient of prestigious Alabama EPSCoR graduate fellowship during his Ph.D. He is a Member of Optica and SPIE.

Rui Zhou (Student Member, IEEE) was born in Lanzhou, China. She received the B.S. degree in electrical engineering and the M.S. degree in optical engineering from China Jiliang University, Hangzhou, China, in 2011 and 2014, respectively. In 2016, she joined the Precision Ultrafast Light Sciences (PULS) Group, University of Alabama in Huntsville, Huntsville, AL, USA, to pursue Ph.D. degree in optical science and engineering. Her research interests include ultrafast optics, ultrafast carrier dynamics in novel semiconductors, and fiber optic sensing. She is a Student Member of Optica.

Lingze Duan (Senior Member, IEEE) received the Ph.D. degree from the University of Maryland, College Park, MD, USA, in 2002. He is currently a Professor with the Department of Physics and Astronomy, University of Alabama in Huntsville (UAH), Huntsville, AL, USA. He was a Postdoctoral Researcher with the Massachusetts Institute of Technology, Cambridge, MA, USA, and Penn State University, State College, PA, USA, before joining UAH in 2007. He has authored or coauthored more than 100 peer-reviewed or refereed technical publications. His research interests include ultrafast optics, ultrafast carrier dynamics in semiconductor materials and devices, precision measurement and spectroscopy, and fiber optics. He was the recipient of the NSF CAREER Award in 2013, UAH Graduate Mentor Award in 2021, and College of Science Outstanding Faculty Award in 2022. He is a Senior Member of Optica.